Journal of Biomedical Optics

BiomedicalOptics.SPIEDigitalLibrary.org

Predictive assessment of kidney functional recovery following ischemic injury using optical spectroscopy

Rajesh N. Raman
Christopher D. Pivetti
Rajendra Ramsamooj
Christoph Troppmann
Stavros G. Demos

SPIE.

Rajesh N. Raman, Christopher D. Pivetti, Rajendra Ramsamooj, Christoph Troppmann, Stavros G. Demos, "Predictive assessment of kidney functional recovery following ischemic injury using optical spectroscopy," *J. Biomed. Opt.* **22**(5), 056001 (2017), doi: 10.1117/1.JBO.22.5.056001.

Predictive assessment of kidney functional recovery following ischemic injury using optical spectroscopy

Rajesh N. Raman,[a,b,*] Christopher D. Pivetti,[c] Rajendra Ramsamooj,[d] Christoph Troppmann,[c] and Stavros G. Demos[a,b,†]
[a]Lawrence Livermore National Laboratory, Livermore, California, United States
[b]University of California, Davis, Center for Biophotonics Science and Technology, Sacramento, California, United States
[c]University of California, Davis Medical Center, Department of Surgery, Sacramento, California, United States
[d]California Northstate University College of Medicine, Elk Grove, California, United States

Abstract. Functional changes in rat kidneys during the induced ischemic injury and recovery phases were explored using multimodal autofluorescence and light scattering imaging. The aim is to evaluate the use of noncontact optical signatures for rapid assessment of tissue function and viability. Specifically, autofluorescence images were acquired *in vivo* under 355, 325, and 266 nm illumination while light scattering images were collected at the excitation wavelengths as well as using relatively narrowband light centered at 500 nm. The images were simultaneously recorded using a multimodal optical imaging system. The signals were analyzed to obtain time constants, which were correlated to kidney dysfunction as determined by a subsequent survival study and histopathological analysis. Analysis of both the light scattering and autofluorescence images suggests that changes in tissue microstructure, fluorophore emission, and blood absorption spectral characteristics, coupled with vascular response, contribute to the behavior of the observed signal, which may be used to obtain tissue functional information and offer the ability to predict posttransplant kidney function. [DOI: 10.1117/1.JBO.22.5.056001]

Keywords: kidney; ischemia; reperfusion; spectral imaging; *in vivo*.

Paper 160677PRR received Sep. 30, 2016; accepted for publication Apr. 4, 2017; published online May 3, 2017.

1 Introduction

Prolonged periods of ischemia can compromise tissue function. Currently, there is no available tool deployable at the time of medical intervention to measure the degree of ischemic injury incurred in tissue or predict the return of its function. An available option is to perform biopsy and histopathologic analysis that help to identify biochemical and microstructural changes in the tissue in response to ischemia. However, tissue sampling is invasive, preparation and analysis can take days to complete, and subtle assessment and prediction of tissue viability based on morphologic changes alone is not possible (unless there is complete tissue necrosis that represents but one extreme end of the spectrum of tissue viability). Hence, tissue sampling for the assessment of viability is not always practical for transplantation or emergency trauma cases. An alternative technology yielding more timely results might be microdialysis, a procedure in which a ~2-mm-wide needle is inserted into the tissue in order to sample the extracellular environment for ischemia by-products. This method, however, is also invasive and can alter local blood flow and tissue metabolism.[1,2] When tissue of critical or unknown status must be assessed, a real-time, noninvasive method is therefore preferred. Consequently, the most prevalent clinical method for estimating the degree of ischemic injury is based on the tissue's general characteristics and history (e.g., patient age, length of ischemic time, presence or absence of other tissue stressors) as well as subjective characteristics such as its visual appearance.

Without a means to decisively determine tissue functional status, one of two unfavorable risks may be run: (1) transplanting dysfunctional tissue can increase the morbidity and mortality of the patient as well as associated medical cost. (2) Discarding functional though poorly perfused tissue fails to maximize the availability of much needed viable kidneys, the organ with the highest discard rate in deceased donor solid organ transplantation.[3] Furthermore, given a more accurate and timely evaluation of tissue function, proper therapeutic decisions could be made, e.g., whether to resuscitate injured tissue in trauma or peripheral vascular disease patients, or whether such a process (with its own inherent risk for the patient) would be futile.

Previous work has suggested that optical spectroscopy methods may be able to provide noninvasive, real-time monitoring of tissue recovery following ischemic injury.[4–6] In these studies, NADH (reduced nicotinamide adenine dinucleotide) fluorescence intensity was found to be correlated to cellular metabolic state. More recently, research has suggested the utility in monitoring multiple parameters during ischemia and reperfusion in order to characterize kidney status.[7] Ultraviolet interrogation of tissue is a superficial interaction due to much higher absorption in the UV by tissue components. Normal kidney function is characterized by filtration of the blood primarily in the cortex or outer region of the kidney. This highly metabolically active region is comprised of tubules, single cell-thick structures where the blood vessels have branched out to the capillaries, and where waste products diffuse from the blood into the filtrate (which later is to become urine and expelled from the body).

*Address all correspondence to: Rajesh N. Raman, E-mail: raman4@llnl.gov

†Current address: University of Rochester, Laboratory for Laser Energetics, Rochester, New York 14623, United States

Filtration depends on specific permeability and cell polarization characteristics of the tubules, which become hypoxic and are compromised during ischemia.[8] In a previous study, we measured that about 85% of the autofluorescence (AF) under 355-nm excitation and about 70% of the AF under 266-nm excitation (which is used only for normalization) was originating from the cortex in rat kidneys.[9] Translating these numbers for the case of a human kidney, where the thickness of the outermost protective capsule layer (comprised of collagenous fibrils embedded with elastin fibers) surrounding the kidney is larger, we estimated that about half of the measured AF under 355-nm excitation should be originating from the cortex while ~90% of AF under 266-nm excitation should be originating from the capsule. These results support our hypothesis that interrogating the kidney superficially under UV excitation can lead to determination of organ-level function.

Our technical approach is also motivated by evidence that a noncontact optical interrogation method is preferred in order to avoid inducing signal artifacts that can arise from various factors when applying pressure on the tissue with a fiber probe, including (1) altering the scattering properties of the tissue during the measurement and (2) introducing pressure-induced *in vivo* local ischemia, which leads to altered optical signatures.[10,11] As a result, this work represents an expansion of historical work using the principle that (1) AF under 355-nm excitation probes NADH and monitors the metabolic response of the tissue and (2) AF under 266-nm excitation arises mainly from tryptophan (a structural fluorophore not involved in metabolism), which provides a reference signal that was demonstrated to correct for signal artifacts from movement and changing distance of the measuring probe to the tissue.[11] Furthermore, AF under 266 nm partially compensates for modulation in the detected signal arising from changes in the induced absorption by blood (though not completely, due to different photon penetration depths at 266 and 355 nm and nonuniform distribution of blood with depth). Analysis of the complex dynamics of the ratio of these two signals indicated strong correlation to the injury time.[11]

In this work, we expand upon these earlier measurements to include additional signals in order to help probe additional aspects of tissue response to better explain the origin of the optical signal dynamics. Specifically, we added to the above AF signals the AF signal under 325-nm excitation, as well as scattering (SC) signals at 355, 325, 266, and 500 nm (480 to 520 nm) to aid in decoupling the various aspects of the complex physiological response associated with perturbing and monitoring an *in vivo* system. These additional signals were generated with the aim to develop a direct relationship between clinically known physiological responses of the kidney (to ischemic injury and reperfusion) to fitting parameters of the signal ratio and the associated kidney dysfunction pathways. 325- and 500-nm wavelengths are isosbestic to the hemoglobin (Hb/HbO_2) oxygenation state and better elucidate the effect of total blood absorption and modification on the excitation delivered to the tissue and emission recorded by the detector. Furthermore, the study included monitoring the animal physiological parameters and clinical outcomes for up to 30 days following ischemia or until death. The results allow for an evaluation of various optical signatures to predict kidney viability and suggest the potential of such a noncontact approach, currently nonexistent, to provide clinically useful information in real time.

2 Methods

2.1 *Rat Preparation*

Subject preparation has been described in detail previously.[12] All animal procedures were approved by the University of California, Davis, Animal Use and Care Administrative Advisory Committee (AUCAAC) and Institutional Animal Care and Use Committee (IACUC). Adult male spontaneously hypertensive rats (SHR) were placed under general anesthesia using 2% isoflurane delivered with 1.0 L of air per minute. Following a midline laparotomy, the kidneys were made accessible for imaging, vascular clamping, and periodic topical saline administration.

2.2 *Renal Ischemia*

Simultaneous arterial and venous flow was temporarily occluded resulting in unilateral ischemic injury to the left kidney, henceforth referred to as the injured kidney. The right kidney was not clamped (normal kidney). Ischemia was induced for either 20 ($n = 9$ rats) or 150 ($n = 10$) min. At the end of the injury phase, the clamp was released and the kidneys were allowed to reperfuse (at least 45 min following a 20-min injury, and at least 60 min following a 150 min injury). Based on our prior studies and the literature, a 20-min kidney ischemia is recoverable in rats, whereas a 150-min injury is expected to be irreversible.[13–15]

2.3 *Optical Imaging*

A schematic of the imaging configuration is shown in Fig. 1(a).[12] Three laser sources provided UV excitation at 355 (UVSQAOM355-5, Meshtel), 266 (DTL-382QT, Power Technology), and 325 nm (HeCd Omnichrome, Melles Griot) with average fluences of 0.2, 0.2, and 2 mJ/cm^2, respectively. In addition, white LED emission filtered by a 500 ± 20 nm bandpass dielectric filter (Corion) provided visible illumination. 325-nm excitation is isosbestic with respect to hemoglobin (Hb) oxygenation, yet also excites NADH (but not tryptophan). The illumination output from these lasers was combined and coupled into a fiber bundle whose output permitted full illumination of both kidneys. The AF and 500-nm SC images were recorded through a 420- to 640-nm band-pass filter combination (GG-420 and BG-38, Schott) positioned in front of the first liquid nitrogen-cooled 16-bit CCD camera (TE/CCD-512-TKM/1, Roper Scientific). This choice of filter was made in order to capture the emission from NADH (centered at ~460 nm) under 355- and 325-nm excitation and the emission tail from tryptophan extending in this region under 266-nm excitation.[16] Laser sources were utilized due to the simplicity in handling the light transport, but LED light sources are currently available and could alternatively have been used. A second identical CCD acquired light scattering images under UV laser excitation. In this case, a 240- to 400-nm bandpass filter (UG-11, Schott) rejected the AF and 500-nm SC components of the collected signal. Sample AF and SC images of the kidneys of the same rat at the start of the experiment are shown in Fig. 1(b) under 355-, 266-, and 500-nm illumination. After these baseline images were taken, the clamp was applied to the kidney on the right and image acquisition resumed. Images under 325-nm illumination looked similar to those under 355-nm illumination.

Intensities from both AF and SC images were measured after a sequence of normalization steps to remove variations in laser

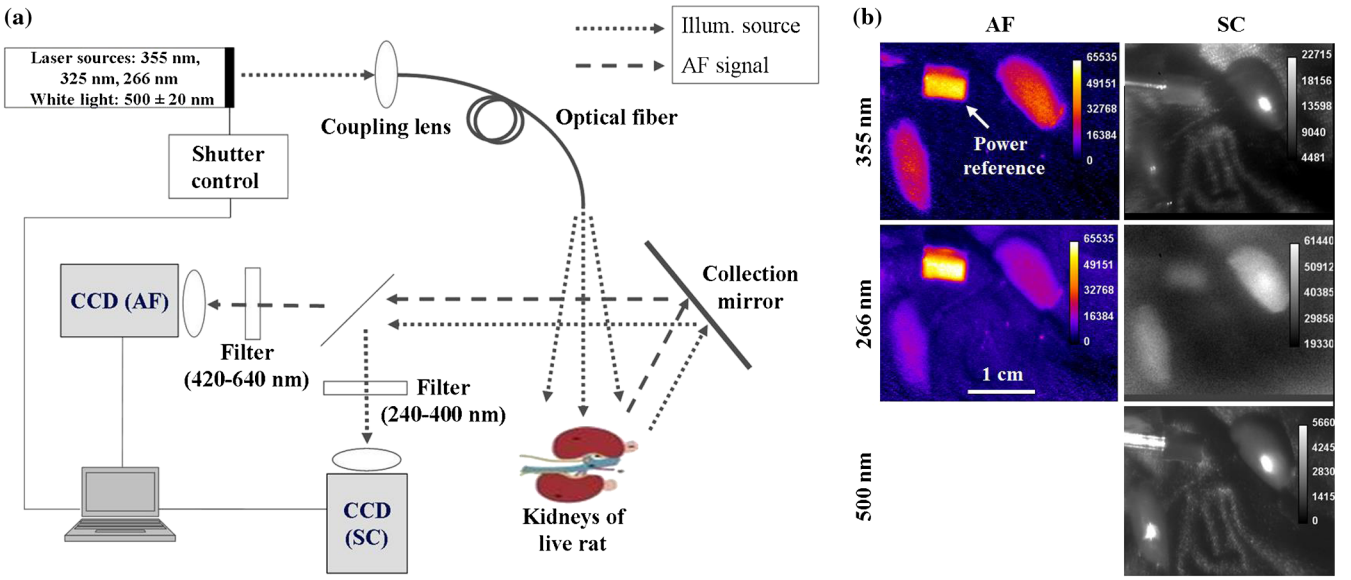

Fig. 1 (a) Schematic of the multimodal spectral imaging experimental setup. (b) Example AF and scattering (SC) images from the same rat prior to clamping the kidney on the right. Labeled intensities are normalized to maximum. Scale bar is common to all images.

fluence both spatially and temporally. Specifically, following subtraction of CCD counts with no illumination present (dark counts, which includes that of stray light present in an otherwise dark room), images of normalized intensity were generated by dividing, pixel-by-pixel, the CCD count in the kidney image by that of a prerecorded beam profile to account for spatial nonuniformity, and then dividing by exposure time of 4 s. The beam profile was collected at the start of the experiment as an image of a sheet of premium quality paper placed in the field where the kidneys are to be located and illuminated under each source for either camera. From each image, regions of interest were defined on the kidney over as large as possible an area (~0.8 cm^2, for assessment of kidney function) as well as on a reference fluorescing (or scattering, depending on the camera) object [Fig. 1(b)] positioned in the illumination field, whose average intensity was used to monitor changes in laser power during image acquisition. Mean CCD count from each kidney was divided by that from the reference object to obtain the normalized kidney intensity. Each temporal trace was normalized to its value at the time just prior to clamping. Specifically for the SC images, the region of the image exhibiting specular reflection (defined as <90% of maximum pixel value) of the incident light was excluded from analysis.

2.4 *Optical Spectroscopy*

AF spectra under 355 nm, UV excitation were collected by imaging onto the slit of a spectrometer (Triax 320, Jobin-Yvon Horiba, equipped with a 300-grooves/mm grating blazed at 450 nm) the emission from a rat kidney during 150 min ischemia and 90 min reperfusion (under the same illumination conditions described in the imaging configuration). A 385-nm long-pass filter (GG-385, Schott) was positioned at the entrance of the spectrometer for 355- and 325-nm excitation and a 295-long-pass (WG-295, Schott) for 266-nm excitation to reject the excitation light from entering the spectrometer. The spectra were detected by a back-illuminated CCD (LN/CCD-1340/400EB/1, Roper Scientific). After correcting for system response, each spectrum was normalized to peak intensity. This normalization was motivated by our interest in observing how the spectral profile itself changes during injury and recovery as well as because animal movement prevented a reliable measurement of absolute emission intensity.

2.5 *Survival Study Protocol and Statistical Analysis*

Following imaging, the normal kidney was removed and the abdominal cavity was sutured closed. Postoperatively, rats were given 0.3 cc buprenorphine (0.2 mg/kg body weight) injection subcutaneously for analgesia. Rat weight, physical appearance, and survival were monitored for 30 days following ischemia, or until a rat lost more than 20% of preoperative body weight (at which time it was sacrificed) or until death. Death from acute renal failure was diagnosed by timing of death, kidney inspection following death, and subsequent histology.

Following death, the injured kidney was removed, fixed in 10% formalin, sliced into sections of subcellular thickness,

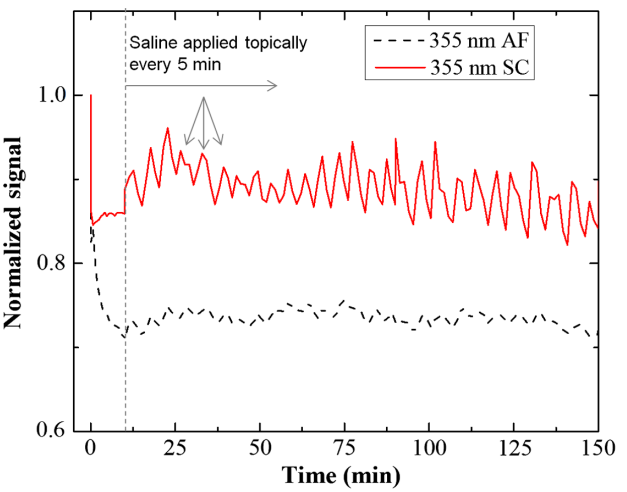

Fig. 2 Plot of fluorescence (dotted) and scattered (solid) signals under 355 nm excitation, averaged over $n = 10$ profiles undergoing 150 min injury.

and stained with hematoxylin-eosin (H&E). The slides were reviewed by a pathologist blind to the experimental group and outcome. The percentages of acute (occurring immediately after injury) and chronic (occurring days to weeks after injury) histologic changes present on each slide were converted into a numerical score as follows: 0 (0%), 1 (<25%), 2 (25% to 75%), and 3 (>75%).

Fisher's exact test was employed to detect differences in survival outcome based on injury time. Histological scores were analyzed with Wilcoxon rank-sum test. Survival was calculated according to Kaplan–Meier. Statistical survival comparisons were made using the Log-rank test. All statistical tests were conducted in custom written software. Rats with a surgical complication as cause of death were censored from survival analysis.

3 Results

Figure 2 shows the 355-nm SC and AF signals as a function of time averaged over all individual profiles obtained during the study using 150 min of injury. Ten minutes into injury, saline was topically applied periodically every 5 min. The SC signal, which has been used as the reference signal when monitoring NADH in earlier studies,[5,17] was extremely sensitive to topical

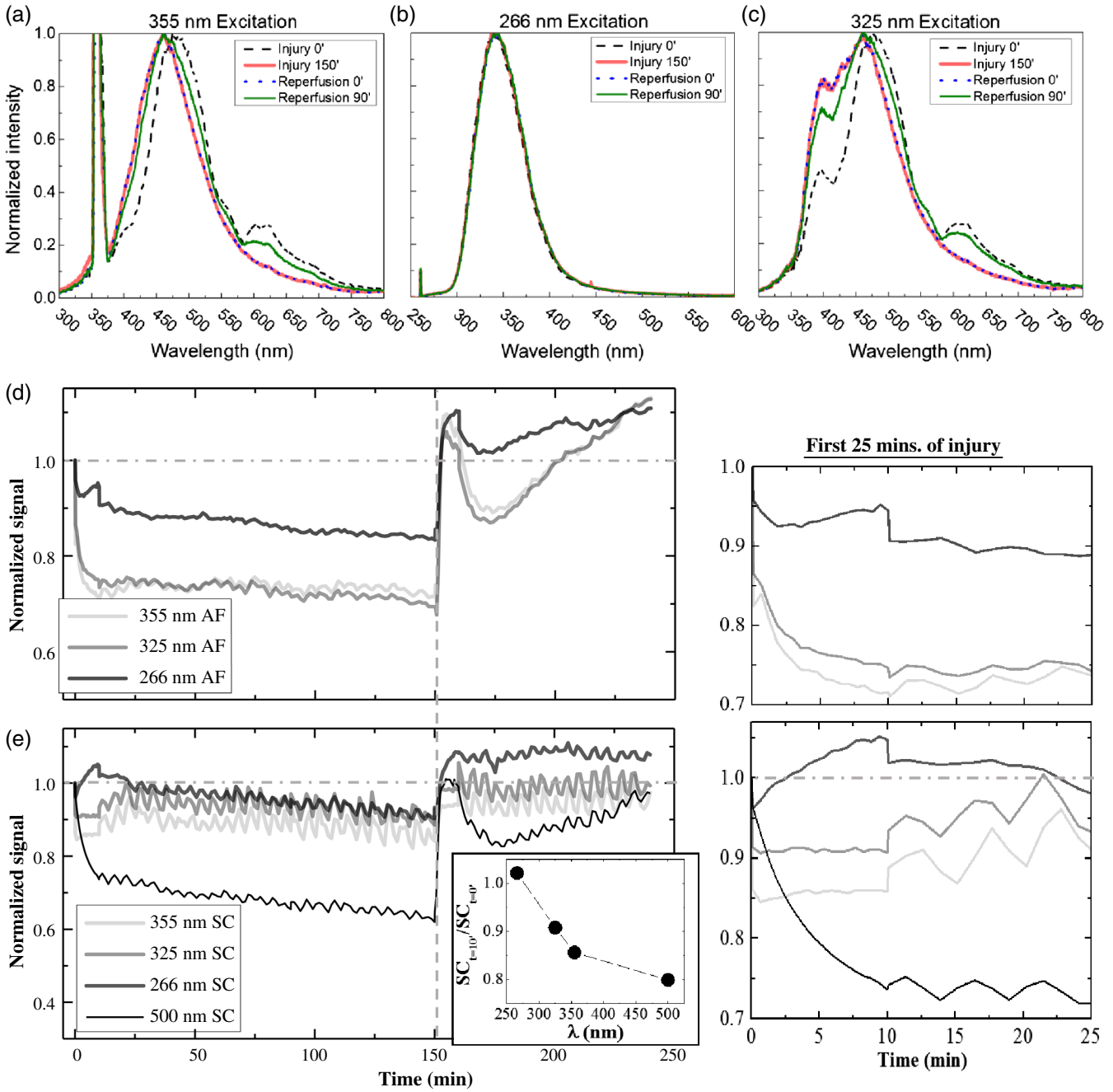

Fig. 3 AF spectra (a–c) of the injured kidney under (a) 355 nm, (b) 325 nm, and (c) 266 nm excitation. (d) AF and (e) scattering signals averaged over $n = 10$ profiles of rat kidneys undergoing 150 min ischemia followed by 90 min reperfusion under various illumination wavelengths. Panels to the right of (d) and (e) show the first 25 min of the traces on left. Inset in (e) shows the wavelength dependence of the scattered signal 10 min into injury.

saline in this noncontact configuration. Specifically, an abrupt signal increase was observed followed by a decrease over the next several minutes (as indicated by the arrows in Fig. 2), while the AF signal was relatively less affected (peak-to-valley of AF signal is only 33% that of the SC signal) by saline application.

The spectra (normalized to peak intensity) under UV excitation are shown in Figs. 3(a)–3(c) at various times during injury and reperfusion. Under 355-nm excitation, the spectrum peaks at 480 nm [Fig. 3(a)] undergoes an apparent blueshift during injury (attributed to modification in absorption by blood in the interrogated volume[18]). Following reperfusion for 90 min, the spectrum returns toward the preinjury profile but does not replicate it. The spectrum under 325-nm excitation [Fig. 3(b)] resembles that under 355 nm at wavelengths above 420 nm (the spectral range used in the imaging experiments) and exhibits an additional component with peak around 390 nm. The spectrum under 266-nm excitation [Fig. 3(c)] did not change appreciably with injury or reperfusion.

Figure 3(d) shows the AF intensities, averaged over all measurements of a rat kidney undergoing 150 min ischemia followed by 90 min reperfusion, under 355-, 266-, and 325-nm excitation. The 355-nm AF signal decreased after prolonged injury and recovered in two phases during reperfusion. It was also observed that the AF signal intensity under 266-nm excitation is significantly less sensitive to injury than that under 355-nm excitation. A signal discontinuity after clamp placement is observed, which is possibly due to the change in the distribution of blood within the vascular system of the kidney. Another discontinuity is observed at the 10 min mark and coincides with the first application of saline. This effect was greater in the signal obtained under 266-nm excitation than under 355-nm excitation. Another observation is that the 325-nm excitation AF signal was nearly identical to that under 355 nm except after prolonged injury when the signals deviated slightly (~7%, see Fig. 4).

Figure 3(e) shows the SC profiles (266, 325, 355, and 500 nm) that were acquired simultaneously with the AF profiles. Apart from the effects of saline and clamping placement, the temporal changes of the 355- and 266-nm SC signals were limited (<10%) during ischemia and reperfusion. Interestingly, the behavior of the 500-nm SC profile (which arises mainly from blood absorption) bears a strong resemblance (but is not identical) to that of the metabolic-related 355-nm AF profile during both injury and reperfusion. The remaining scattering profiles exhibited similar (but smaller) changes, especially at the onset of reperfusion. These results are suggesting that absorption of the emission under UV excitation by blood is influencing the observed AF signal. These observations prompted the exploration of additional signal normalization methods.

Figure 4 shows profiles of various signal ratios. Specifically, the AF signal under 355-nm excitation is normalized by the (a) AF signal under 266-nm excitation (abbreviated 355AF/266AF), (b) 500-nm SC signal (355AF/500SC), and (c) AF signal under 325-nm excitation (355AF/325AF). The 355AF/325AF normalized profile shows very small changes with time along with a gradual but definite differential response during injury, which is reversed during reperfusion. This is not surprising as the emission generated by both excitations originated mainly from the same species (NADH). On the other hand, the 355AF/266AF and 355AF/500SC profiles exhibit a rapid change at the onset of the reperfusion phase but with characteristic differences in the response observed in each profile. These behaviors will be discussed in more detail in the next section.

3.1 *Results of Fitting the Reperfusion Signals to Model*

Figure 5(a) shows a sample fit of the 355AF/266AF ratio during reperfusion of a rat subjected to 20 min ischemia according to an empirical double exponential model given by the product of the following two components:[11]

$$\text{Component 1}: R_N = \begin{cases} R_{\text{NO}} & t_r < t < \Delta\tau \\ R_{\text{NO}} - \Delta R_N \times [1 - \text{Exp}(-(t-\Delta\tau)/\tau_N)] & t < \Delta\tau \end{cases}, \quad (1)$$

$$\text{Component 1}: R_E = R_{E0} + \Delta R_E \times [1 - \text{Exp}(-t/\tau_E)], \quad (2)$$

where t_r denotes the start of reperfusion, $\Delta\tau$ is the delay time of component R_N, τ_N is its relaxation time, τ_E is the relaxation time of R_E, R_{N0}, and R_{E0} are the values of the first signal ratio data point upon reperfusion, and ΔR_N and ΔR_E represent the magnitude of decrease and increase, respectively, of the first and second components. Equation (1) models the expected behavior of [NADH], in which [NADH] decreases as oxygenated blood supply, and thus the main oxidation pathway is restored.[19] Equation (2) models the modulation affecting the measured signal by environment factors to be discussed later.

To evaluate the ability of the 500-nm SC signal to predict kidney recovery, fitting parameters characterizing the dynamics of the 500-nm SC signal (related to the ability of the tissue to

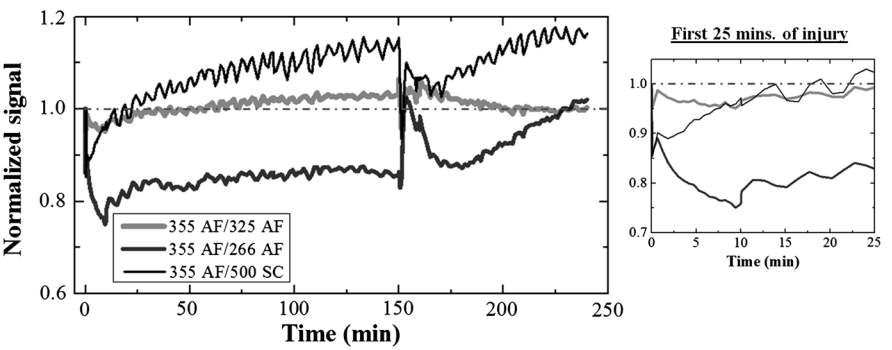

Fig. 4 Various signal ratio profiles involving the 355-nm excitation AF signal. Panel to the right shows the first 25 min of the traces on the left.

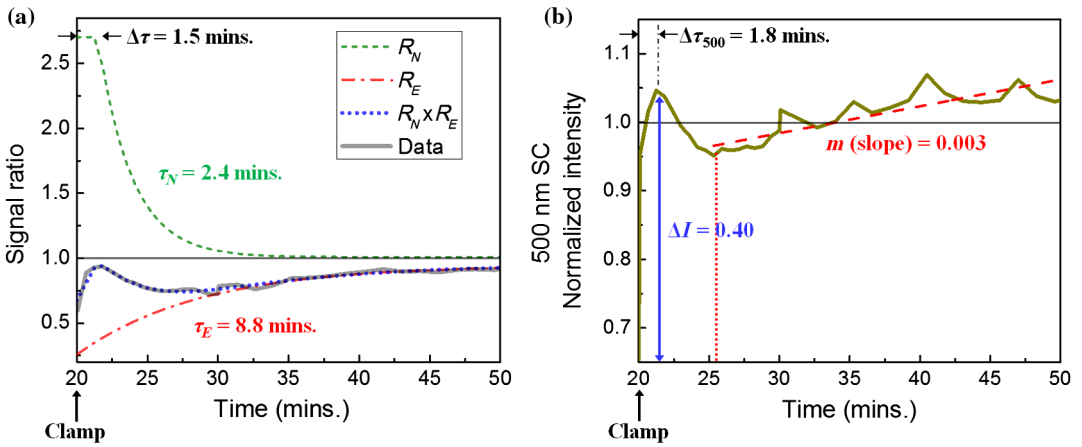

Fig. 5 Example of parametrization of (a) 355-nm AF/266-nm AF and (b) 500-nm SC signals obtained from the reperfusion phase of a rat following 20 min of renal ischemia. See text for parameter definitions.

clear a hypothesized modification that affects absorption by blood, such as blood coagulation byproducts and/or blood concentration) were likewise obtained. These features [Fig. 5(b)] are (1) intensity change ΔI representing the change in intensity from clamp release to first peak, (2) peak delay $\Delta\tau_{500}$ representing the delay time associated with ΔI, and (3) recovery slope m representing the rate of recovery from the subsequent local minimum (dotted vertical line) to the end of the optical monitoring period and obtained by linear regression.

3.2 *Survival Outcome*

Figure 6 summarizes the results of the survival portion of the study including (a) survival rate over the course of the monitoring period and (b) acute and chronic histology scores following autopsy. One death in the 20 min group was attributed to unintentional ischemia of the bowel during the experiment and its data were excluded from statistical analysis and above plots. By day 7, survival rate for the 150 min group was 0% while at the end of the monitoring period, survival rate for the 20 min group was significantly greater at 90% (Fisher's exact test, $p < 0.0001$). The median acute histology score was higher (by one point, or up to 25% histologic changes) in nonsurvivors than in survivors, indicating more severely injured kidneys in the former group and, as also evidenced by the clinical course, strongly suggestive that the cause of death was indeed renal failure.

3.3 *Comparison of AF and 500-nm SC Results to Survival Outcome*

Figure 7 compares the values of the time constants based on injury time. Significantly longer time constants from 355AF/266AF signal ratio were associated with the longer injury (two-sample t-test, $p < 0.01$) [Fig. 7(a, left)], consistent with previous studies.[11] When comparing time constants based on survival outcome (i.e., if injury time were not known, as is often the case in clinical transplantation), it was found for all three time constants that nonfunctional kidneys yielded larger values than functional kidneys (two-sample t-test, $p < 0.01$) [Fig. 7(a, right),]. Results of parametric fits from the 500-nm SC signal are summarized in Fig. 7(b). In this signal, only $\Delta\tau_{500}$ and m from the 500-nm SC signal were good predictors of survival ($p < 0.01$ for both parameters, and where an inverse correlation was found for the latter with survival).

Figure 8 shows photographs of the kidneys of two rats to help appreciate the difference of visual observation with the results of the signal ratio analysis. Figure 9 displays the individual values of the fit parameters (summarized in Fig. 7) derived from the signal ratio [Fig. 9(a)] and the 500-nm SC [Fig. 9(b)], including those for the two rats depicted in Fig. 8. The injured kidney following 20 min of injury shown in Fig. 8(a) looks similar in color and visual perception to the injured kidney following 150 min of injury shown in Fig. 8(c) (although the latter has a tint of chocolate brown, not well represented in the color photograph). Similarly, both injured kidneys shown in Figs. 8(b) and 8(d)

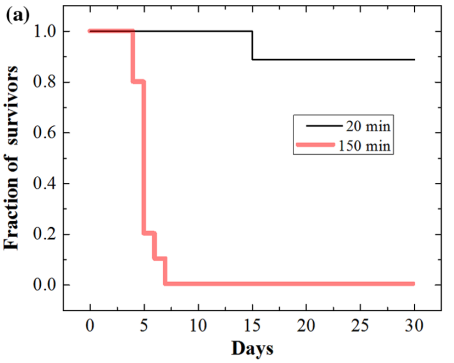

(b)

	MEDIAN HISTOLOGY SCORES			
	Acute		Chronic	
	30-Day survivors	Non survivors	30-Day survivors	Non survivors
20 min ischemia	0	1	0	0
150 min ischemia	-	1	-	0

Fig. 6 Survival outcome summary. (a) Survival rate for rats with 20 min versus 150 min warm renal ischemia. (b) Acute and chronic histology scores at autopsy.

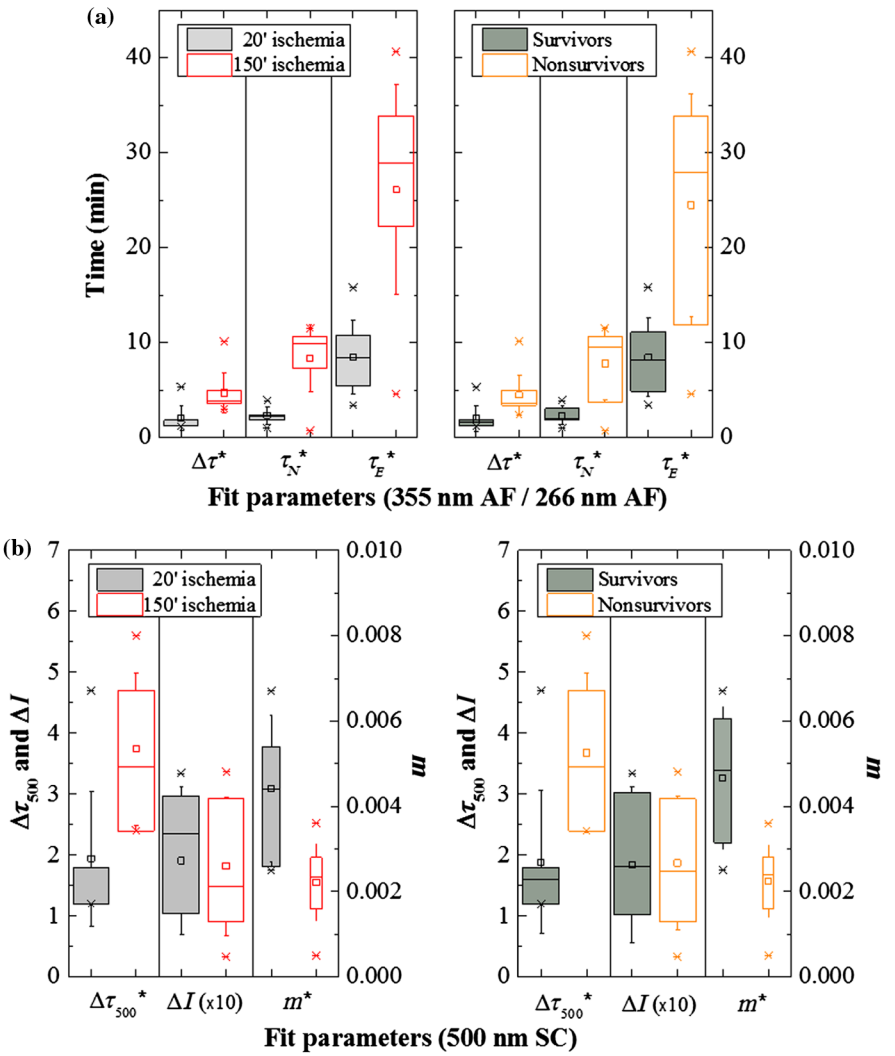

Fig. 7 Box plot (range: 25th and 75th quartiles. Whiskers: 1 SD) of parameters from (a) 355-nm AF/266-nm AF signal ratio and (b) 500-nm SC signal grouped by injury time (left) versus survival outcome (right). *Parameters exhibiting a significant difference ($p < 0.01$).

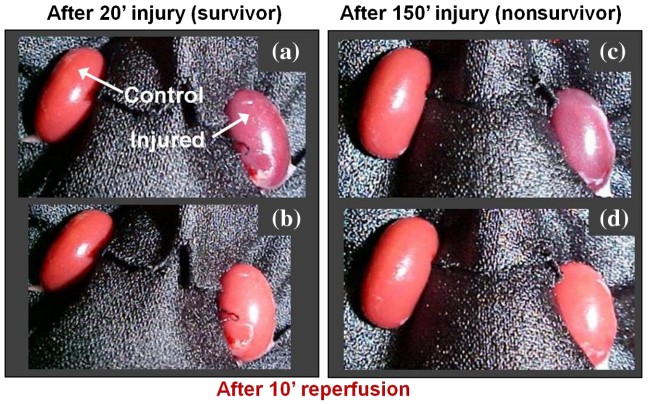

Fig. 8 Kidneys of two live rats (left column and right column) under anesthesia resting on a black cloth covering the abdomen. Injured kidneys (on the right in each photograph) are shown at the end of the specified injury phase in (a) and (c), the clamp in place under the cloth. Kidneys are shown again 10 min after reperfusion in (b) and (d) following specified duration of injury.

appear identical after 10 min of reperfusion and resemble the normal kidneys as well (and remained as such throughout reperfusion). The rat in Figs. 8(c) and 8(d) succumbed to renal failure.

Figure 9(a) displays a three-dimensional plot of the individual values of the three time constants of each injured kidney (including the two depicted in Fig. 8) derived from the signal ratio that were summarized in Fig. 7(a), separated by survival outcome. The value of each data point is feature-scaled by subtracting each value from the mean of the sample set and then dividing by the standard deviation. In this manner, parameters in different units can be compared. The corresponding normalized parameter values derived from the 500-nm SC signal are shown in Fig. 9(b). These plots provide a visualization of the normalized parameter space that may be used to predict the function of an ischemically injured kidney. In each panel of Fig. 9, two arrows indicate the location in the parameter space of the two visually nearly identical (after 10 mins. of reperfusion) injured kidneys in Fig. 8, showing that these kidneys are clearly distinguishable using five of the six proposed parameters. The Euclidean distance δ between the two kidneys using either the signal ratio or 500-nm SC alone is labeled on each panel of Fig. 9. In this calculation, ΔI was excluded

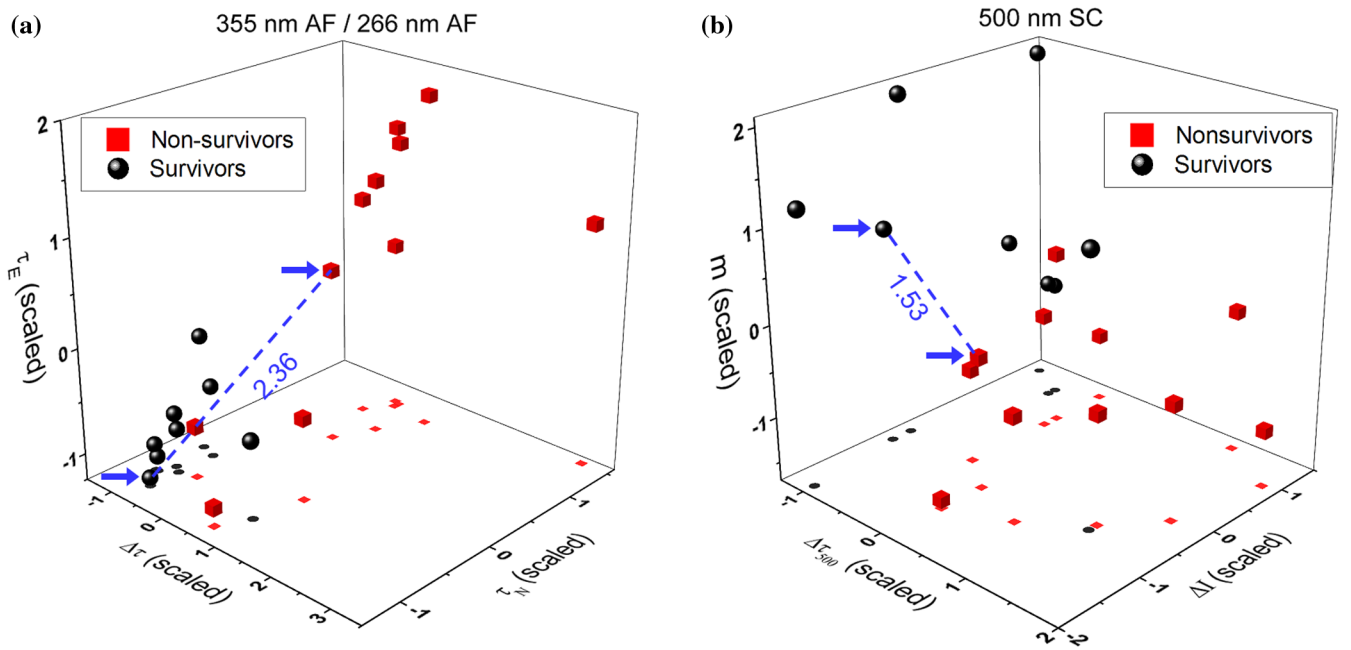

Fig. 9 Individual values of the fit parameters obtained from signal ratio profile of (a) 355 nm AF/266-nm AF and from (b) the 500-nm SC profile summarized in Figs. 7(a) and 7(b), separated by survival outcome. Values are feature-scaled (mean-subtracted and normalized by standard deviation). Arrows indicate the time constants of the two injured rat kidneys shown in Fig. 8. Numbers between these data points indicate the Euclidean distance.

since it exhibited no statistically significant sensitivity to survival. In doing this, we find that $\delta_{355AF/266AF} = 2.36$ whereas $\delta_{500SC} = 1.53$. This result says that the AF signal ratio alone provides 54% more discriminating power than that of the 500-nm SC alone and emphasizes the value in employing UV excitation (or a combination of both).

4 Discussion

In this study, we explore the ability of fitting parameters to the dynamic temporal profile of optical signals to identify kidneys unlikely to recover from injury. Timing of death (i.e., clinical course), autopsy, and histology (only available days after the injury proves fatal), all confirmed that kidneys subject to 150 min of ischemia were nonrecoverable. Our optically based determination is made with data available within the initial 10's of minutes of reperfusion. This can translate in a clinical setting to an optical evaluation method that can be employed while the organ recipient is still on the operating table—or perhaps even prior to that time as significant recent advances in the area of kidney graft preservation have led to the initial clinical implementation of *ex vivo* normothermic organ perfusion. With the latter preservation modality, kidneys are placed—after recovery from the deceased donor and initial cold storage—on an *ex vivo* pump circuit. The kidneys are then perfused under near-physiologic normothermic (37°C) conditions with blood, thus allowing not only for organ preservation but also for assessment, potential intervention(s), and reconditioning prior to deciding whether to proceed with transplantation.[20] *Ex vivo* perfusion therefore also constitutes an ideal setting for our optical tissue assessment method as on one hand, it provides a (post-reperfusion) setting that replicates the one encountered in a recipient (which is required to perform our measurements), but on the other hand does not require that a recipient undergo a potentially futile transplantation surgery (had the organ been predicted to be nonviable and require immediate removal after reperfusion has occurred).

The scattering signals demonstrate that topical saline administration, a clinical standard to ensure adequate tissue hydration, introduces artifacts. Specifically, the signal increases significantly when saline is applied, and then as the moisture evaporates or is absorbed into the tissue the signal decreases. This effect arises from changes in the scattering properties of the tissue surface and mainly the backscattered signal that is collected by our imaging system. The origin of this effect is outside the scope of this work and will not be further discussed.

The spectra confirm that the AF under 355- and 325-nm excitation are dominated by NADH emission. The spectral profiles obtained under 325- and 355-nm excitation at wavelengths longer than about 420 nm are practically identical and follow the same changes as a function of injury and reperfusion time as exemplified by the four different time points shown in Figs. 3(a) and 3(b). On the other hand, the AF spectra under 266-nm excitation are dominated by tryptophan emission while the spectral profiles remain practically unchanged during injury and reperfusion. It should be mentioned that the AF spectra under 325- and 355-nm excitation contain emission from additional intrinsic fluorophores. In Ref. 9, we argued that these additional fluorophores (such as collagen and elastin) are structural components, which should not respond to changes in cell metabolism and instead would present an additional static signal on top of the temporally changing signal during ischemia and reperfusion. In addition, our biexponential model relies on temporal changes of the 355-nm AF/266 nm AF ratio, and not the magnitudes of the signal changes, during reperfusion to extract the time constants presented in this study.

The 355-nm AF signal itself exhibited a decrease after prolonged injury that is not explained with a simple model of emission intensity based solely on [NADH] [Eq. (1)]; it has long been

known that oxygen deprivation increases tissue [NADH][5,21] and should therefore lead to an increase in emission intensity. Conversely, a signal decrease is expected during reperfusion, yet the observed signal exhibits a more complex and multiphase recovery. In particular, the 355AF/266AF ratio profile exhibits a rapid increase for a time $\Delta\tau$ after the clamp is released, followed by a decrease and subsequent recovery associated with a slower increase described by relaxation constants τ_N and τ_E. To explain the physiological basis of these behaviors, one needs to consider the changes in the absorption and scattering properties of the tissue at both the excitation and emission wavelengths and the underlying biological responses, specifically those that contribute to the signal model "environment" component (represented by τ_E) of Fig. 5(a). Known tissue responses to ischemia that could affect the optical properties of the tissue include change in concentration of absorbers, creation or destruction of absorber species, change in their quantum yield, and change in the size, shape, and scattering efficiency of cellular and subcellular components. The plurality of excitation wavelengths and their corresponding monitored signals employed in this work were part of our effort to help separate out individual possible processes and investigate the underlying mechanisms.

Although the pathophysiology of renal ischemia/reperfusion injury is not completely understood, the involvement of a number of dynamic processes is generally accepted, including endothelial and epithelial cell injury and altered renal vascular function with ensuing hemodynamic changes.[22] The initial injury further initiates an inflammatory response that can lead to reduction in local blood flow to the renal cortex (which is accessed by the optical methodology employed in this work) and outer medulla, with debilitating consequences for tubular function and viability.[8,23,24] This vascular congestion compounds the hypoxic conditions and further reduces the ability to clear the toxic-free radicals and lactic acid during reperfusion whose removal would be expected to result in the contraction of vasculature (dilated during hypoxia and elevated acidosis) back toward its physiological state. Below, we interpret the observed signals in the context of the known pathophysiology of ischemia and reperfusion injury.

The recorded dynamics of the optical signal during the very early injury phase is associated with basic pathophysiologic consequences such as change in the blood pressure (and resulting changes in blood flow and response of the tissue surface) and reduction of blood oxygenation. These observations are therefore valuable in that they can help separate the optical signal changes that result from these early processes from the more complex responses occurring after prolonged injury and during the reperfusion phase.

We begin first by analyzing the light scattering signals. During the initial five min of warm kidney ischemia, the scattering signal at all wavelengths is observed to decrease with time. The scattering signal represents the fraction of the illumination that is backscattered after interacting with the tissue. The interaction with the tissue involves mainly two processes: (a) the diffuse scattering of the illumination and (b) the attenuation of the illumination due to absorption (mainly by blood) inside the tissue. Therefore, the initial decrease of the light scattering signal can be assigned to changes in the absorption properties of the tissue (blood) and changes in the light scattering properties of the tissue. For both mechanisms, the penetration depth of the light in the tissue as a function of wavelength is of critical importance.

As scattering originates at each wavelength from different penetration depths, the effect of blood concentration as a function of the depth and ensuing changes due to the obstruction of the blood flow are strongly influencing the measured scattering signals. The kidney is covered by the renal capsule, a thin membranous sheath composed of tough fibers, chiefly collagen and elastin. The capsule receives its blood supply from the interlobar arteries, small vessels that branch off from the main renal arteries, travel through the cortex of the kidney, and terminate in the capsule. It is within these microvessels where absorption of the excitation (and emitted light) is likely occurring, especially at 266-nm excitation. Below the capsule, the blood supply and concentration in the cortex region will affect predominantly the 500-nm SC signal (as the penetration depth at 500 nm is much larger than under UV excitation and is estimated to be on the order of 1 mm for rat kidney tissue) as well as the AF and SC signals under 325- and 355-nm excitation (we assume that the penetration depth at 325 nm is closer to that at 355 nm). Thus, the expected penetration depth at these wavelengths is monotonic with wavelength.

The results shown in the inset of Fig. 3(e) after 10 min of tissue injury indicate that the relative reduction of the scattering signal is also monotonic with wavelength. This change cannot be attributed to the deoxygenation of the blood as 325 and 500 nm are isosbestic points in the absorption spectra of oxy- and deoxyhemoglobin. It must be noted that 500 nm is not an isosbestic point for methemoglobin (metHb), as discussed next in more detail. However, there should be no metHb production within the early stages of the injury. We therefore assign this change to an increase in the blood concentration in the outer region of the tissue governed by three main mechanisms. First, after renal pedicle clamping, renal microvessels may dilate faster and more profoundly in response to hypoxic conditions in the more metabolically active outer cortical region than in the more central regions of the kidney. As a result, there may be passive redistribution of the intrarenal blood and a net increase of the tissue blood content in the areas where blood vessels are more dilated. Second, when clamping the renal pedicle, some or all of the juxtarenal macrotributaries of the renal vein such as the adrenal vein, gonadal vein, and large lumbar veins may not necessarily be clamped. As a result, in the minutes following the renal pedicle clamping, there may be some passive flow of blood out of the kidney into any of these patent tributaries as the increased pressure in the entire kidney's arterial macro- and microvasculature at the moment of clamping would be expected to equalize with the pressure in the venous system after clamping—yielding a net egress of fluid out of the kidney and resulting in a loss of tissue turgor (and a collapse of the tissue). Third, since the ureter is not clamped during these experiments, the kidney continues to produce urine over at least the first few of minutes of ischemia, resulting in further net loss of fluid. These three effects may cause shrinkage of the kidney, resulting initially in an increased blood and tissue concentration (mass density) in the outer region of the kidney interrogated by the light. The net effect manifests as a decrease in the observed SC signal as a result of increased absorption by blood components.

This reduction of the kidney volume would then also cause a densification of the capsule, which in turn should contribute to increased scattering of the light, particularly at 266 nm. This effect may initially be masked by the change in the blood concentration within the kidney (vide supra), which causes

increased absorption and reduction of the overall backscattered signal. However, as the blood concentration is rebalanced by diffusion and gravity, which causes migration of blood toward the dependent portion of the kidney (i.e., the side opposite to the imaged kidney side), the concentration of blood within the interrogated tissue volume decreases and the scattering signal starts recovering. Consistent with the above discussion, this recovery is stronger for the 266-nm SC signal and weaker for the 500-nm SC signal.

The origin of the subsequent wavelength-independent slow decrease of the SC signals after about 25 min in the injury phase is possibly more complex. We postulate that this behavior again is arising from blood, which causes changes of the absorption coefficient. Because blood is depleted of oxygen within about 20 min, as confirmed by cross-polarized red light scattering (Ref. 25, see discussion below on 325 nm signal), and is accompanied by a change in the color of the kidney from bright red to deep maroon, changes in scattering observed during prolonged ischemia may more likely include blood coagulation and production of metHb, a known byproduct of ischemia. metHb is known to have a higher absorption coefficient than Hb in the visible/red spectrum[26] and may be responsible for the chocolate brown color (darkening) of the kidneys at the end of prolonged injury. In addition, the very early stages of inflammation could also affect the measured optical signals after sufficient exposure of the organ to ischemic injury (on the order of 30 min or longer), but the extent of their potential contribution to the dynamics of the optical signal observed during the injury phase is at this point uncertain. These processes are also affecting the spectral profiles of the emission as shown in Figs. 3(a) and 3(b). For example, the lack of the characteristic spectral features in the emission spectra after 150 min of ischemia under 355 nm (or 325 nm) excitation in the 500- to 600-nm spectral region, which are expected to arise from absorption by either Hb or HbO, may be assigned to the dominant presence of metHb within the blood volume.

A rapid increase in the scattering signal is observed immediately after reperfusion. The 266-nm SC signal returns to above baseline levels (normalized signal = 1) and remains above baseline for the duration of our observed reperfusion phase. Based on the arguments presented above, this behavior of the 266-nm SC signal may be indicative that the reperfusion did not fully restore the physical and other characteristics of the capsule that it had prior to the onset of the ischemic injury. This assumption is also suggested by the emission spectra under 325- and 255-nm excitation where, as noted earlier, the spectral profiles after reperfusion remain different from those before the initiation of injury. This observation may at least in part be due to microvascular and pericapillary edema (arising from the ischemic injury) in the capsular region that prevents full restoration of blood flow (and of net capsule blood content) to preinjury levels. Irreversible capsular modification may be verifiable by histology, though definitive elucidation of the mechanism that underlies our observations awaits further study. As a result, the lower absorption of the 266-nm excitation light by blood in the capsule region contributes to enhanced backscattered signal. On the other hand, the 355- and 325-nm SC signals return to baseline and remain near baseline values during the reperfusion phase. The 500-nm SC signal exhibits a more complex behavior, initially returning to baseline (after reperfusion) but then subsequently declining again, suggestive of longer-term relaxation phenomenon. This complex behavior of the 500-nm SC signal is assigned to the change in blood concentration and relative contribution in the absorption by metHb. Previous work[18] suggests that metHbO is becoming dominant in the absorption spectrum of the blood after about 30 min of ischemia.

The above analysis of the temporal evolution of the SC signals provides useful information to interpret the tissue AF results. The AF temporal profiles under all employed excitation wavelengths resemble that of the 500-nm SC profile, which in turn also suggests that they are at least partly influenced by changes in blood absorption/reabsorption within the near surface volume where the UV excitation localizes. However, these profiles are not identical, as is demonstrated by the temporal profiles of the various ratio signals, which exhibit significant variations and provide additional information of the processes involved. This issue is discussed in more detail next.

The 355AF/325AF ratio of Fig. 4 helps elucidate the role of blood oxygenation in the observed AF signals. Due to the close proximity of the two wavelengths, NADH is excited by both wavelengths and their penetration depth is similar. As a result, the difference in the signal ratio arises from the difference in the extinction of the excitation due to absorption by blood. At 325 nm, both HbO and Hb exhibit lower absorption than at 355 nm with coefficient $\alpha(\mathrm{HbO}, 325\ \mathrm{nm}) \approx 0.86\ \alpha(\mathrm{HbO}, 355\ \mathrm{nm})$ and $\alpha(\mathrm{Hb}, 325\ \mathrm{nm}) \approx 0.63\alpha(\mathrm{Hb}, 355\ \mathrm{nm})$.[27] The relatively smaller absorption of Hb at 325 nm causes increased emission under 325-nm excitation as the blood is enriched with Hb and consequently a decline in the 355AF/325AF ratio in the first 15 min as observed in the data. This characteristic response of blood deoxygenation immediately following clamp placement causes reduction in this signal ratio and the reverse behavior during reperfusion. In both cases, the signals respond within minutes.[25] Additionally, after the initial ~20 min of injury we see a slow reversal in this behavior in the 355AF/325AF ratio profile.

The initial decline in the 355AF/500SC ratio at the onset of ischemic injury reverses earlier than the decline of the individual constituent profiles and within the time window that the reversal of the UV scattering signals was observed. Furthermore, as 500 nm is an isosbestic point for Hb, this signal is largely unaffected by change in blood oxygenation. This may indicate that the origin of this behavior is associated with the initial increase of the blood concentration, a response that was also suggested earlier in relation to the temporal behavior of the scattering signals. The subsequent increase of the 355AF/500SC ratio with progression of injury may arise from the formation of metHb, which exhibits much stronger absorption at 500 nm compared to both Hb and HbO.[26] The 355AF/500SC ratio returns to baseline upon reperfusion but subsequently exhibits a behavior that more closely follows the 355AF/266AF ratio.

While the 355AF/266 AF ratio profile has been argued to relate to metabolic activity of the tissue, the 500-nm SC profile is related to the blood content in the tissue that is being assessed. The underlying putative pathophysiological mechanisms of the observed correlation of fit parameters, obtained from both the 355AF/266AF signal ratio and (for comparison) the 500-nm SC signal, with kidney dysfunction are considered next.

After release of the clamp, the 500-nm SC signal initially increases as shown in Fig. 3(e). We hypothesize that this behavior is dictated by removal of metHb and other blood byproducts upon the onset of the flow of fresh oxygenated blood. This removal process varies within kidney vessels depending on

their size and distance from the main blood supply. In addition, the vessels (which had dilated over the course of the injury in response to hypoxia and increasing levels of acidosis) begin to contract, further contributing to an increase in scattering signal (via reduced absorption). The parameter ΔI from the start of reperfusion to its first peak represents a quantification of the amount of signal change due to the hemodynamics. This parameter varied significantly from case to case within the same group and, therefore, was a poor discriminator of kidney function. Subsequently, the decrease of the 500-nm SC signal from this peak may be assigned to changes in the blood concentration as well as changes in the tissue absorption in the cortex region of the kidney (which can be reached by the 500 nm light) as a result of the initiation of reperfusion injury (including inflammation) from rapid introduction of fresh oxygen to damaged tissue and ensuing generation of free radicals. The blood concentration can be affected by the vasculature diameter, which may start increasing again following its initial rapid contraction after reperfusion as in a damped oscillator. The signal then relaxes to its final state (characterized by a recovery rate m) as the overall measured tissue and vascular response progresses toward steady-state. Smaller m values were found to be associated with longer injury times, suggesting that longer injuries manifest with slower recoveries in the 500-nm SC signal. Figure 7(b, right) shows $\Delta\tau_{500}$ and m to be good predictors of survival.

Turning our attention to the 355AF/266AF ratio, longer $\Delta\tau$ delay and τ_N relaxation times, thought to be derived primarily from the alteration of the dynamics of NADH emission, could be due to breakdown in the electron transport chain. This complex multistep process, responsible for the generation of important energy-storing molecules, may require more time to respond to new oxygenated blood during reperfusion after a more severe injury. The fit parameter τ_E was a good predictor of kidney failure, suggesting that injury-associated pathophysiological alterations may have been responsible for its behavior. One possible environmental factor may involve modulation of NADH emission by blood absorption, in particular the delay in restoring normal blood volume or normal mixture of optically absorbing blood components. A second factor may involve the emission of the NADH fluorophore itself. Substances such as lactic acid may be responsible during injury for reducing NADH quantum efficiency and decreasing emission intensity. This can be due to an increase in tissue pH,[21,28] for example. This would also explain our observation of a strong correlation of the optical properties of the injured tissue after reperfusion with the severity of the preceding injury. Protein-bound NADH is primarily found inside the double membraned mitochondria, and lactic acid is a by-product of glycolysis occurring in the cytoplasm. One of the first cellular changes that result from a disruption of the ATP production is the loss of cellular and organellular membrane integrity. The resulting increased membrane permeability may acidify the local environment of bound NADH and thereby decrease its emission yield. Another potential explanation for a reduction in NADH emission efficiency during injury is the dissociation of NADH from mitochondrial enzyme complexes.[29] In healthy cells, these complexes mediate electron transfer from NADH. However, in injured cells, NADH may dissociate as mitochondrial integrity declines.

Although the exact mechanisms that underlie the observed signal changes during and after ischemia are still speculative, the majority of the derived fitting parameters offer an advantage over visual perception. From the photographs in Fig. 8, it is apparent that while visual observation cannot readily distinguish a kidney subjected to 20 min of injury from one subjected to 150 min injury, either after injury or after 10 min of reperfusion, analysis of the 355AF/266AF ratio and 500-nm SC signals yield distinct values (excepting ΔI) for the time constants (arrows in Fig. 9). The delay in tissue optical response in the case of prolonged injury is associated with high probability of kidney failure. Therefore, our results suggest that these two optical signals (the signal ratio more so than the 500-nm SC) are directly related to the degree of the ischemic tissue injury and of the ensuing pathophysiological response and may have predictive value regarding the clinical outcome.

5 Conclusion

In this work, multimodal imaging during kidney ischemic injury and reperfusion provided information relating to tissue function. Namely, analysis of the temporal behavior of the signal ratio formed by dividing the AF under 355 nm to that under 266 nm has shown that kidneys injured irrecoverably respond during reperfusion with statistically significantly slower AF dynamics. This information can be used to predict kidney failure when visual observation cannot, and it can be used to do so almost immediately following the injury phase. In addition, multimodal imaging has provided insights into various physiological events, which may be occurring during ischemia and reperfusion, that are responsible for the observed behavior of the signal ratio. Results indicate that absorption of the emission by blood dominates over scattering effects and is likely due to vascular response to injury and reperfusion and the possible generation of metHb. Additionally, blood oxygenation state has minimal influence on the dynamics of the signal ratio throughout the injury and recovery processes.

Disclosures

The authors have no financial interests and no other potential conflicts of interest to disclose in this manuscript.

Acknowledgments

This work was performed under the auspices of the U.S. Department of Energy by Lawrence Livermore National Laboratory under contract DE-AC52-07NA27344. This work was supported in part by funding from the Center for Biophotonics, an NSF Science and Technology Center, managed by the University of California, Davis, under Cooperative Agreement No. PHY 0120999.

References

1. T. Sommer and J. F. Larsen, "Detection of intestinal ischemia using a microdialysis technique in an animal model," *World J. Surg.* **27**, 416–420 (2003).
2. A. Mehrabi et al., "Experimental monitoring of hepatic metabolism by microdialysis glucose, lactate, and glutamate during surgical preparation of the liver hilus," *J. Surg. Res.* **105**, 128–135 (2002).
3. A. O. Ojo et al., "Organ donation and utilization in the USA," *Am. J. Transplant.* **4**, 27–37 (2004).
4. B. Chance, "Spectrophotometry of intracellular respiratory pigments," *Science* **120**, 767–775 (1954).
5. B. Chance et al., "Intracellular oxidation-reduction states in vivo," *Science* **137**, 499–508 (1962).
6. S. Kobayashi et al., "Microfluorometry of oxidation-reduction state of the rat kidney in situ," *J. Appl. Physiol.* **31**, 693–696 (1971).
7. A. Mayevsky et al., "Real-time assessment of organ vitality during the transplantation procedure," *Transplant. Rev.* **17**, 96–116 (2003).

8. L. C. Racusen, "Pathology of acute renal failure: structure/function correlations," *Adv. Renal Replacement Ther.* **4**, 3–16 (1997).
9. R. N. Raman et al., "Evaluation of the contribution of the renal capsule and cortex to kidney autofluoresence intensity under ultraviolet excitation," *J. Biomed. Opt.* **14**(2), 020505 (2009).
10. R. Reif et al., "Analysis of changes in reflectance measurements on biological tissues subjected to different probe pressures," *J. Biomed. Opt.* **13**(1), 010502 (2008).
11. R. N. Raman et al., "A non-contact method and instrumentation to monitor renal ischemia and reperfusion with optical spectroscopy," *Opt. Express* **17**, 894–905 (2009).
12. R. N. Raman et al., "Optical spectroscopy approach for the predictive assessment of kidney functional recovery following ischemic injury," *Proc. SPIE* **7561**, 756109 (2010).
13. R. N. Raman et al., "Factors influencing rat survival in a warm renal ischemia model: time to adapt the protocols," *Transplant. Proc.* **43**, 1511–1514 (2011).
14. A. Ozden et al., "Cytoprotective effect of trimetazidine on 75 min warm renal ischemia-reperfusion injury in rats," *Eur. Surg. Res.* **30**, 227–234 (1998).
15. T. Hayama et al., "Beneficial effect of neutrophil elastase inhibitor on renal warm ischemia-reperfusion injury in the rat," *Transplant. Proc.* **38**, 2201–2202 (2006).
16. R. R. Alfano and Y. Yang, "Stokes shift emission of human tissue and key biomolecules," *IEEE J. Sel. Top. Quantum Electron.* **9**, 148–153 (2003).
17. J. M. C. C. Coremans et al., "Pretransplantation assessment of renal viability with NADH fluorimetry," *Kidney Int.* **57**, 671–683 (2000).
18. R. N. Raman et al., "Quantification of in vivo autofluorescence dynamics during renal ischemia and reperfusion under 355 nm excitation," *Opt. Express* **16**, 4930–4944 (2008).
19. R. Rhoades and R. Pflanzer, *Human Physiology*, 3rd ed., Saunders College Publishing, Fort Worth, Texas (1996).
20. S. A. Hosgood et al., "*Ex vivo* normothermic perfusion for quality assessment of marginal donor kidney transplants," *Br. J. Surg.* **102**, 1433–1440 (2015).
21. A. Mayevsky and B. Chance, "Intracellular oxidation-reduction state measured in situ by a multichannel fiber-optic surface fluorometer," *Science* **217**, 537–540 (1982).
22. T. A. Sutton, C. J. Fisher, and B. A. Molitoris, "Microvascular endothelial injury and dysfunction during ischemic acute renal failure," *Kidney Int.* **62**, 1539–1549 (2002).
23. J. V. Bonventre, *Management of Acute Kidney Problems*, Chapter 2.1, Springer-Verlag, Berlin (2010).
24. R. Munshi, C. Hsu, and J. Himmelfarb, "Advances in understanding ischemic acute kidney injury," *BMC Med.* **9**, 1–6 (2011).
25. J. T. Fitzgerald et al., "Realtime assessment of *in vivo* renal ischemia using laser autofluorescence imaging," *J. Biomed. Opt.* **10**(4), 044018 (2005).
26. W. G. Zijlstra, A. Buursma, and W. P. Meeuwsen-van der Roest, "Absorption spectra of human fetal and adult oxyhemoglobin, de-oxyhemoglobin, carboxyhemoglobin, and methemoglobin," *Clin. Chem.* **37**, 1633–1638 (1991).
27. S. L. Jacques, "Optical properties of biological tissues: a review," *Phys. Med. Biol.* **58**, R37 (2013).
28. T. Eklund et al., "Interstitial lactate, inosine, and hypoxanthine in rat kidney during normothermic ischaemia and recirculation," *Acta Physiol. Scand.* **143**, 279–286 (1991).
29. H. D. Vishwasrao et al., "Conformational dependence of intracellular NADH on metabolic state revealed by associated fluorescence anisotropy," *J. Biol. Chem.* **280**, 25119–25126 (2005).

Rajesh N. Raman received his BA degree in physics from the University of California, Berkeley and his PhD in engineering applied science from the University of California, Davis. He has been a scientist at Lawrence Livermore National Laboratory within the physical and life sciences directorate performing research in support of the National Ignition Facility since 2009. His research interests include developing diagnostics for the detection and characterization of defective optical materials and dysfunctional tissue.

Christopher D. Pivetti received his bachelor's degree in general biology in 2001 and his master's degree in general biology in 2004 from the University of California, San Diego. He is a scientist in the Department of Surgery, UC California Davis Health in Sacramento, California. He serves as the laboratory supervisor and oversees the daily operations of five principle investigators. His research interests include using stem cell therapy to treat congenital anomalies such as spina bifida and diaphragmatic hernia.

Rajendra Ramsamooj received his MD from the University of Minnesota and completed his residency at Stanford University. He is a professor and assistant dean of curriculum at the California North State University College of Medicine. His interests include graduate medical education, tumor biomarkers, and novel imaging techniques.

Christoph Troppmann is an abdominal transplant surgeon and a professor of surgery at the University of California, Davis, School of Medicine in Sacramento, California. He completed his residency training in general surgery followed by fellowship training in transplantation surgery and immunology at the University of Minnesota in Minneapolis, Minnesota. His clinical and research interests include ischemia–reperfusion injury and maximization of marginal deceased donor organ utilization to address the ongoing donor organ shortage.

Stavros G. Demos received his PhD in physics from the City University of New York in 1993. He is currently a senior scientist at the Laboratory for Laser Energetics, University of Rochester. He had previously served as a staff scientist at Lawrence Livermore National Laboratory in parallel to holding research scientist positions at the University of California, Davis Medical Center. His research interests are in the fields of laser–matter interactions, laser-induced damage, and biomedical photonics.